JACS
JOURNAL OF THE AMERICAN CHEMICAL SOCIETY
Communication
pubs.acs.org/JACS

# Lanthanide-Doped $Na_xScF_{3+x}$ Nanocrystals: Crystal Structure Evolution and Multicolor Tuning

Xue Teng,[†] Yihan Zhu,[‡] Wei Wei,[†] Shuchao Wang,[†] Jingfeng Huang,[§] Rafik Naccache,[∥] Wenbo Hu,[#] Alfred Iing Yoong Tok,[§] Yu Han,[‡] Qichun Zhang,[§] Quli Fan,[#] Wei Huang,[#] John A. Capobianco,[∥] and Ling Huang*[,†]

[†]School of Chemical and Biomedical Engineering, Nanyang Technological University, 70 Nanyang Drive, Singapore 637457

[‡]Advanced Membranes and Porous Materials Center, King Abdullah University of Science and Technology, Thuwal 23955-6900, Kingdom of Saudi Arabia

[§]School of Materials Science and Engineering, Nanyang Technological University, 50 Nanyang Avenue, Singapore 639798

[∥]Department of Chemistry and Biochemistry and Centre for Nanoscience Research, Concordia University, 7141 Sherbrook Street West, Montreal, QC, Canada H4B 1R6

[#]Key Laboratory for Organic Electronics & Information Displays (KLOEID) and Institute of Advanced Materials (IAM), Nanjing University of Posts & Telecommunications (NUPT), 9 Wenyuan Road, Nanjing 210046, Jiangsu, China

Supporting Information

**ABSTRACT:** Rare-earth-based nanomaterials have recently drawn considerable attention because of their unique energy upconversion (UC) capabilities. However, studies of $Sc^{3+}$-based nanomaterials are still absent. Herein we report the synthesis and fine control of $Na_xScF_{3+x}$ nanocrystals by tuning of the ratio of oleic acid (OA, polar surfactant) to 1-octadecene (OD, nonpolar solvent). When the OA:OD ratio was increased from low (3:17) to high (3:7), the nanocrystals changed from pure monoclinic phase ($Na_3ScF_6$) to pure hexagonal phase ($NaScF_4$) via a transition stage at an intermediate OA:OD ratio (3:9) where a mixture of nanocrystals in monoclinic and hexagonal phases was obtained and the coexistence of the two phases inside individual nanocrystals was also observed. More significantly, because of the small radius of $Sc^{3+}$, $Na_xScF_{3+x}$:Yb/Er nanocrystals show different UC emission from that of $NaYF_4$:Yb/Er nanocrystals, which broadens the applications of rare-earth-based nanomaterials ranging from optical communications to disease diagnosis.

Upconversion (UC), which is characterized by the successive absorption of several pump photons followed by emission of the output radiation at a wavelength shorter than the pump wavelength, was formulated independently by Auzel and Ovsyankin in the mid-1960s.[1] The UC mechanism can be divided into four broad classes: excited-state absorption, energy transfer, photon avalanche, and the recently discovered energy-migration-mediated UC.[2] Normally combinations of different mechanisms are responsible for various UC processes, and all of these processes involve the sequential absorption of two or more photons and require multiple metastable energy levels in the host materials for efficient energy transfer.[2] Because of their partially filled 4f orbitals, tripositive lanthanide ions possess a multitude of electronic energy states spanning the near-IR (NIR) to UV range, making them ideal host lattices for UC emission studies.[3]

Although UC emission has been observed in various lanthanide-based host materials, including oxides, phosphates, and vanadates,[2,4] fluorides have obtained the most attention because of their intrinsically low phonon energies, which translates into a decrease in the nonradiative relaxation rate that impacts the UC efficiency.[2,5] For example, $NaYF_4$ nanoparticles doped with $Er^{3+}$ (for NIR to green or red) or $Tm^{3+}$ (for NIR to UV, blue or NIR) ions, very often combined with $Yb^{3+}$ as a sensitizer, have shown excellent UC efficiencies and promising applications in lighting, bioimaging, and fine-tuning of the UC emission fluorescence.[2,5] In the rare-earth family, both $Y^{3+}$- and $Ln^{3+}$ ($La^{3+}$, $Ce^{3+}$, $Pr^{3+}$, $Nd^{3+}$, $Sm^{3+}$, $Eu^{3+}$, $Gd^{3+}$, $Tb^{3+}$, $Dy^{3+}$, $Ho^{3+}$, $Er^{3+}$, $Tm^{3+}$, $Yb^{3+}$, and $Lu^{3+}$)-based nanomaterials have been synthesized as host matrices for various applications.[2,4,6] However, scandium, which is found at the very top of group IIIB in the periodic table and has been historically classified as a rare-earth element,[1,2] also sits at the very beginning of the transition-metal series, and its distinct atomic electron configuration may produce optical properties different from those of $Y^{3+}$/$Ln^{3+}$-based nanocrystals. To the best of our knowledge, except for one report using $Sc^{3+}$ as a dopant,[7] studies of the synthesis and optical properties of $Na_xScF_{3+x}$-based host crystal lattices have not been reported to date.

Herein we report for the first time the controlled synthesis of sodium scandium fluoride ($Na_xScF_{3+x}$) nanocrystals doped with different lanthanides via the modified thermal coprecipitation method,[8] in which oleic acid (OA) was used as a polar surfactant and octadecene (OD) as a nonpolar solvent.[9] We found that the phase and composition of the nanocrystals are very sensitive to the polarity of the reaction medium. They changed from pure monoclinic phase ($Na_3ScF_6$) to pure hexagonal phase ($NaScF_4$) when the polarity was increased

**Received:** February 18, 2012
**Published:** April 16, 2012

   dx.doi.org/10.1021/ja3016236 | J. Am. Chem. Soc. 2012, 134, 8340−8343

from low to high, via a core/shell-structured $Na_3ScF_6/NaScF_4$–$Na_3ScF_6$ transition stage at intermediate polarities (Scheme 1).

**Scheme 1. Schematic Illustration of the Crystal Structure Evolution at Varying Polarities of the Reaction Medium (i.e., OA:OD Ratios)**

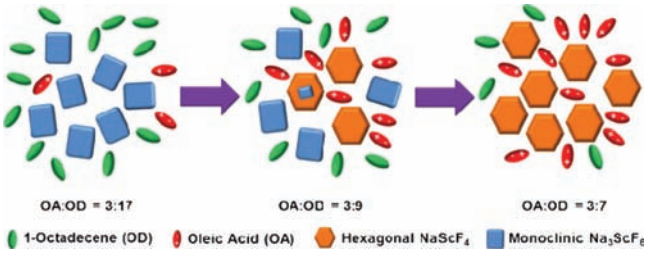


This type of crystal evolution has not been reported previously, nor has it been observed for $Y^{3+}/Ln^{3+}$-based nanocrystals even at the same OA:OD ratios. More importantly, $Na_xScF_{3+x}$ nanocrystals show strong red UC emission (660 nm) when doped with $Yb^{3+}$ and $Er^{3+}$, while $NaYF_4$:Yb/Er nanocrystals usually give strong green UC emission (520–540 nm).

As shown in Scheme 1, we selected three typical OA:OD ratios of 3:17, 3:9, and 3:7, representing low, intermediate, and high polarities of the reaction medium, respectively, to illustrate the details of the crystal structure evolution. Compositional analysis of the nanocrystals using energy dispersive X-ray spectroscopy (EDX) confirmed the presence of the dopant elements Yb, Er, and Tm in the $Na_xScF_{3+x}$ nanocrystals (Figure S1 in the Supporting Information).

Low-magnification transmission electron microscopy (TEM) images show (1) that $Na_xScF_{3+x}$ nanocrystals synthesized at low and high polarities have very uniform sizes of ca. 36 (Figure 1a) and 27 nm (Figure 1g), respectively and (2) that both of the uniform morphologies observed in the low- and high-polarity products appeared in the product at intermediate polarity (3:9) (Figure 1d). High-resolution TEM images indicate that the fringe distances ($d$ spacing) in nanocrystals synthesized at low and high polarities are 0.29 (Figure 1b) and 0.65 nm (Figure 1h), respectively. The fast Fourier transform (FFT) patterns shown in Figure 1c,i can be indexed as monoclinic $Na_3ScF_6$ and hexagonal $NaScF_4$, respectively, on the basis of the their (020)/($\bar{2}$02) and ($1\bar{2}\bar{1}$)/(110) reflections, consistent with their powder X-ray diffraction (XRD) data (Figure S2). At intermediate polarity, we observed not only the physical mixture of monoclinic $Na_3ScF_6$ and hexagonal $NaScF_4$ nanocrystals (Figure 1d) but also the coexistence of the two phases inside individual nanocrystals, i.e., an intermediate structure associated with the phase transition between monoclinic $Na_3ScF_6$ and hexagonal $NaScF_4$ (Figure 1e and Figure S2). Lattice fringes associated with the [$5\bar{3}1$] and [$\bar{1}10$] projections observed in the FFT diffractogram (Figure 1f) further confirmed the presence of both the monoclinic and hexagonal phases, which form a core/shell architecture of the nanocrystals.

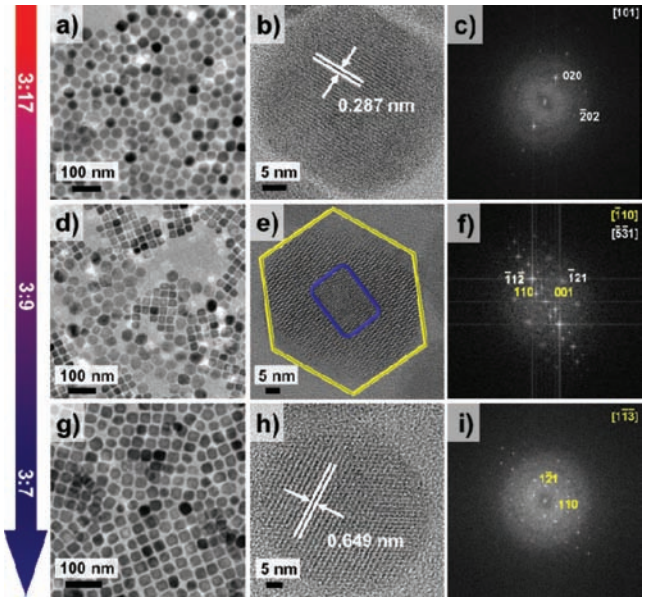


**Figure 1.** (a, d, g) Low- and (b, e, h) high-resolution TEM images and (c, f, i) FFT data for $Na_xScF_{3+x}$ nanocrystals synthesized at OA:OD ratios of (a–c) 3:17, (d–f) 3:9, and (g–i) 3:7. The yellow and blue regions in (e) refer to the crystal structures in the hexagonal and monoclinic phases, respectively.

Further reconstruction of the (001) and (110) lattice fringes of $NaScF_4$ (Figure 2a) revealed a perfect $Na_3ScF_6/NaScF_4$ lattice match along the [001]* direction [$d_{(001)} = 3d_{(1\bar{2}1)}$]. In addition, we observed the presence of Moiré fringes (Figure 2b) resulting from the mismatch at the interface of the ($\bar{1}1\bar{2}$) and (110) lattice planes of $Na_3ScF_6$ and $NaScF_4$, respectively. The measured Moiré fringe spacing ($d_m$ = 1.812 nm) was used to calculate the angle between the involved two sets of lattice planes [$\Phi_{(\bar{1}1\bar{2})/(110)} = 17.7°$], which coincides well with the measured angle between the [$\bar{1}1\bar{2}$]* and [110]* vectors in Figure 1f ($\Phi_{[\bar{1}1\bar{2}]*/[110]*} = 17.2°$). This provides additional support for the proposed $Na_3ScF_6/NaScF_4$–$Na_3ScF_6$ core/shell architecture model.

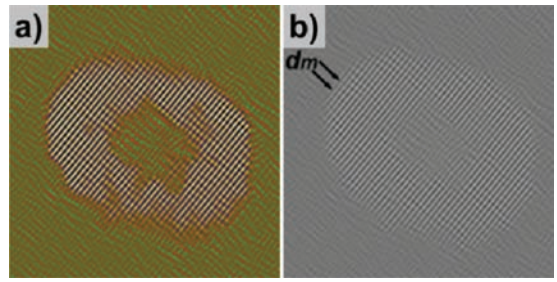


**Figure 2.** (a) Dispersion of the hexagonal phase reconstructed using the (001) and (110) lattice fringes in Figure 1f. (b) Observed lattice fringe of the shell with Moiré fringes.

The TEM results demonstrated that changing the solvent polarity from low to high by increasing the OA content induces the evolution of pure monoclinic $Na_3ScF_6$ nanocrystals to pure hexagonal $NaScF_4$ nanocrystals. This is first triggered by the direct bonding or etching of the strongly coordinative OA ligands,[10] after which the surface crystal structure of $Na_3ScF_6$ is transformed to that of hexagonal $NaScF_4$, which then further extends deep into the nanocrystal. In other words, the OA/OD solvent pair allows us successfully to control the crystal structure between the pure monoclinic $Na_3ScF_6$ and pure hexagonal $NaScF_4$ phases, with the core/shell structure as the transition stage.

This crystal structure evolution could also be monitored by tracking the changes in the XRD patterns of the respective nanocrystals (Figure S2). All of the notable reflections in the


dx.doi.org/10.1021/ja3016236 | J. Am. Chem. Soc. 2012, 134, 8340–8343

XRD patterns can be perfectly assigned to monoclinic $Na_3ScF_6$ and hexagonal $NaScF_4$, and the intensities of the peaks assigned to the hexagonal phase increase remarkably as the OA:OD ratio increases, confirming that the crystal structure evolution occurred as the polarity of the reaction medium changed. At intermediate polarity (Figure S2c), the appearance of XRD signals from both the monoclinic and hexagonal phases indicates the coexistence of the two phases in the product.

To exclude the contribution of reaction time to the crystal structure evolution, we prolonged the reaction time to 3 h from normally 1 h at the intermediate polarity, and almost identical XRD patterns were obtained from these two samples (Figure S3). This clearly proves that it is indeed the polarity of the reaction medium rather than the reaction time that affects the structure and chemical composition of the $Na_xScF_{3+x}$ nanocrystals.

To investigate the effect of the crystal phase on the UC emission, fluorescence spectra were collected on $Na_3ScF_6$, mixed-phase $Na_3ScF_6/NaScF_4$, and $NaScF_4$ nanocrystals, all doped with Yb/Tm/Er ions. Comparison of the three UC spectra in Figure 3a reveals that the positions of the three

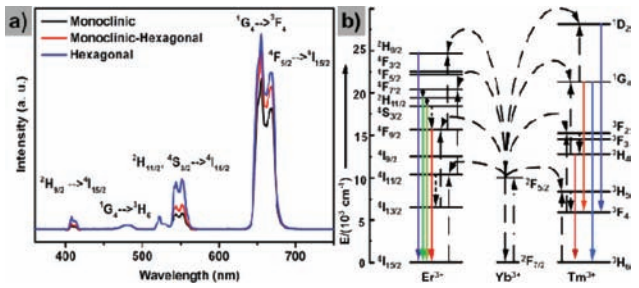


**Figure 3.** (a) UC fluorescence spectra of $Na_xScF_{3+x}$:Yb/Tm/Er (18/0.2/2 mol %) nanocrystals in pure monoclinic, mixed monoclinic/hexagonal, and pure hexagonal phases. (b) UC energy transfer mechanisms of the nanocrystals.

emission peaks remained unchanged and that the dominant transition is $^4F_{9/2} \rightarrow {}^4I_{15/2}$. However, the overall UC intensity increased as the nanocrystals changed from monoclinic to the monoclinic/hexagonal mixture and further to the pure hexagonal phase. This change in UC emission intensity is reminiscent of the trend observed in $NaYF_4$:Yb/Er nanocrystals as the crystal phase changes from cubic to hexagonal.[2] This is due to the presence of two independent sites for both $Yb^{3+}$ and $Er^{3+}$, which quadruples the number of possible $Yb^{3+}$ to $Er^{3+}$ energy transfer processes.[11] Figure 3b depicts the details of the UC energy transfer mechanisms.

Figure 4 shows the remarkable difference in the red/green (R/G) ratios of the UC fluorescence spectra of hexagonal-phase $NaScF_4$:Yb/Er and $NaYF_4$:Yb/Er nanocrystals. In contrast to $NaYF_4$:Yb/Er nanocrystals, which generally give a very small R/G ratio (1:13; Figure 4b), $NaScF_4$:Yb/Er nanocrystals show a very large R/G ratio (6:1; Figure 4a). This dramatic R/G ratio change is also reflected by the different colors of their respective solutions (Figure 4 insets), under 980 nm laser excitation. Therefore, unlike the $NaYF_4$:Yb/Er nanocrystals with strong green UC emission, this novel $NaScF_4$ nanocrystal provides a new and efficient rare-earth-based nanophosphor with strong red UC emission (660 nm), which could find applications, for example, in multiplexing.

The remarkable difference in the R/G ratios for $NaYF_4$:Yb/Er and $NaScF_4$:Yb/Er may be attributed to the difference in the

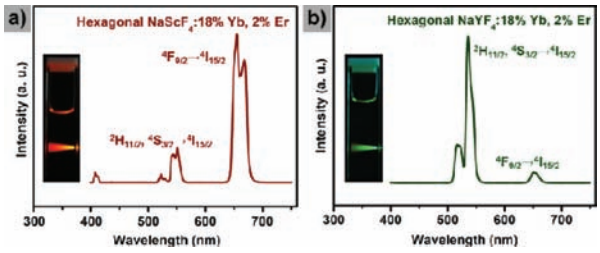


**Figure 4.** UC fluorescence spectra of hexagonal-phase (a) $NaScF_4$:Yb/Er and (b) $NaYF_4$:Yb/Er nanocrystals. The insets show the UC emission colors of the respective nanocrystals in cyclohexane solution.

ionic radii of $Sc^{3+}$ (0.83 Å) and $Y^{3+}$ (1.06 Å), which results in much shorter $Sc^{3+}$–$Sc^{3+}$ distance relative to that of $Y^{3+}$–$Y^{3+}$ when present in the similar fluoride-bridged moieties inside the host lattice structure. Consequently, the doping of $Er^{3+}$ and $Yb^{3+}$ into the $Na_xScF_{3+x}$ host structure by substitution of $Sc^{3+}$ cations creates closer $Er^{3+}$–$Yb^{3+}$ cation pairs than in $Y^{3+}/Ln^{3+}$-based nanocrystal lattices. On the other hand, it is important to note that introducing $Ln^{3+}$ cations into the framework of $Na_xScF_{3+x}$ nanocrystals could also induce strong structural inhomogeneity due to the large difference in the cationic radii of $Sc^{3+}$ and $Ln^{3+}$, probably in the form of $Ln^{3+}$ clustering. This phenomenon has also been recently reported in a $NaYF_4$:Gd system by van Veggel and co-workers,[12] where the difference in the ionic radii is much smaller than that in the $NaScF_4$ host.

It is well-known that the superexchange effect of the lanthanide dimers through their bridging ligands dominates the fast energy transfer for UC emission.[13] Within the same bridging mode, the cross-relaxation effects of lanthanide dimers can be directly compared from their different separations. The shorter distance between $Er^{3+}$ and $Yb^{3+}$ cations in $Na_xScF_{3+x}$ remarkably enhances the cross-relaxation between them, which diminishes the population in the $^2H_{11/2}$ and $^4S_{3/2}$ levels and enhances the population in the $^4F_{9/2}$ energy level of $Er^{3+}$. As a result, the observed red emission is much stronger than the green emission (Figure 4a), which is contrary to what is observed for the $\beta$-$NaYF_4$ host nanophosphors (Figure 4b). The UC fluorescence emission in Figure 4a proves that the same principle is also applicable to $NaScF_4$:Yb/Er nanocrystals.

To achieve further UC emission color tuning, we synthesized $NaScF_4$ nanocrystals tridoped with $Yb^{3+}/Tm^{3+}/Er^{3+}$ ions at varying $Er^{3+}$ concentrations. It is evident from Figure 5b that increasing the concentration of $Er^{3+}$ from 0 to 2.0 mol % caused dramatic changes in the intensities of the three characteristic peaks at 410, 550, and 660 nm, resulting in clearly visible color changes from royal-purple to pinkish-purple in their solutions (Figure 5a), under 980 nm laser excitation. Figure 5c shows that as the $Er^{3+}$ concentration increased from 0.5 to 2.0 mol %, the intensities of the peaks at 410, 550, and 660 nm increased by factors of 19, 11, and 36, respectively.

This result proves the importance of the $Er^{3+}$ concentration in tuning the UC emission color. It also suggests that the energy transfer process becomes more efficient as the $Er^{3+}$concentration increases, which was confirmed by the increased intensities of all the UC emission peaks. Meanwhile, higher $Er^{3+}$ concentration also makes the total fluorescence emission more characteristic of $Er^{3+}$ rather than $Tm^{3+}$, whose characteristic peaks appear when the $Er^{3+}$ concentration is 0 mol % (Figure 5b). The detailed energy UC mechanism is shown in Figure 3b.


dx.doi.org/10.1021/ja3016236 | J. Am. Chem. Soc. 2012, 134, 8340–8343

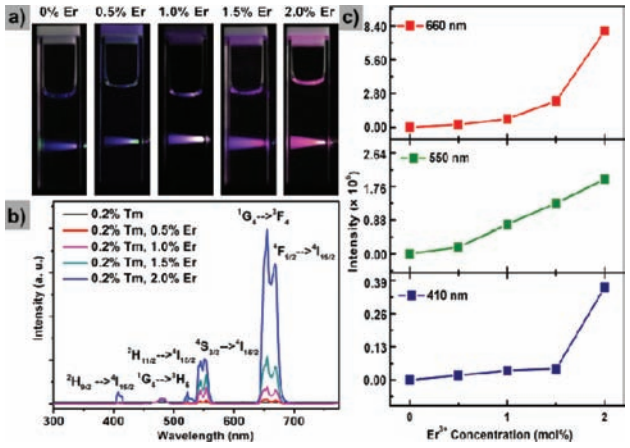


**Figure 5.** (a) Digital photos of $NaScF_4$:Yb/Tm/Er nanocrystals containing different $Er^{3+}$ concentrations in cyclohexane solution. (b) UC fluorescence spectra of $NaScF_4$:Yb/Tm/Er (18/0.2/$x$ mol %) nanocrystals in which the $Er^{3+}$ concentration ($x$) increased from 0 to 2.0 mol %. (c) Intensity changes in the three characteristic emission peaks at 660, 550, and 410 nm as functions of $Er^{3+}$ concentration.

We further synthesized hexagonal-phase $NaScF_4$ nanocrystals doped with other lanthanide ions (e.g., $Sm^{3+}$, $Eu^{3+}$, $Tb^{3+}$, $Dy^{3+}$, $Pr^{3+}$) for downconversion luminescence studies. TEM images (Figure S4a,c,e,g,i) showed (1) that the nanocrystals are ∼24 nm in size and have very uniform morphology, resembling those of Yb/Tm/Er-doped $NaScF_4$ nanocrystals, (2) that the synthetic strategy is widely applicable to $NaScF_4$ nanocrystals doped with other rare-earth elements, and (3) that the low-concentration doping does not alter the nanocrystal growth process. Characteristic downconversion luminescence spectra were also collected for these nanocrystals with different dopants (Figure S4b,d,f,h,j), which can be used as nanophosphors in multiple labeling and disease diagnosis.

In summary, unlike those of $Y^{3+}$/$Ln^{3+}$-based nanocrystals, a unique relationship between the phase and structure of $Na_xScF_{3+x}$ nanocrystals and the polarity of the reaction medium was discovered, on the basis of which uniform nanocrystals of pure monoclinic $Na_3ScF_6$, a superimposed $Na_3ScF_6$/$NaScF_4$–$Na_3ScF_6$ core/shell architecture, or pure hexagonal phase $NaScF_4$ can be easily synthesized. More significantly, the small radius of $Sc^{3+}$ results in a new nanophosphor exhibiting efficient red UC emission (660 nm), which further complements the exploration of rare-earth-based nanomaterials for a wide variety of applications including display, solar energy, catalysis, bioimaging, and telecommunications.

## ■ ASSOCIATED CONTENT

### Supporting Information

Experimental details for the synthesis of doped $Na_xScF_{3+x}$ nanocrystals and analytical data including EDX, XRD, TEM, and fluorescence spectra. This material is available free of charge via the Internet at http://pubs.acs.org.

## ■ AUTHOR INFORMATION

### Corresponding Author

LHuang@ntu.edu.sg

### Notes

The authors declare no competing financial interest.

## ■ ACKNOWLEDGMENTS

L.H. is grateful for the financial support from the Nanyang Technological University Start-Up Grant (SUG) and the Ministry of Education Tier One Grant (RG20/09). J.A.C. holds a Concordia University Research Chair in Nanoscience and is grateful to Concordia University and the Natural Sciences and Engineering Research Council (NSERC) of Canada for financial support of his research. R.N. thanks NSERC for financial support through the Alexander Graham Bell Graduate Scholarship Program.

## ■ REFERENCES

(1) (a) Auzel, F. *J. Lumin.* **1966**, *45*, 341. (b) Feofilov, P. P.; Ovsyankin, V. V. *Appl. Opt.* **1967**, *6*, 1828. (c) Auzel, F. *Chem. Rev.* **2004**, *104*, 139.

(2) (a) Bünzli, J.-C. G.; Eliseeva, S. V. *J. Rare Earths* **2010**, *28*, 824. (b) Haase, M.; Schäfer, H. *Angew. Chem., Int. Ed.* **2011**, *50*, 5808. (c) Yan, Z.-G.; Yan, C.-H. *J. Mater. Chem.* **2008**, *18*, 5046. (d) Wang, F.; Liu, X. *Chem. Soc. Rev.* **2009**, *38*, 976. (e) Wang, G.; Peng, Q.; Li, Y. *Acc. Chem. Res.* **2011**, *44*, 322. (f) Binnemans, K. *Chem. Rev.* **2009**, *109*, 4283. (g) Bogdan, N.; Vetrone, F.; Ozin, G. A.; Capobianco, J. A. *Nano Lett.* **2011**, *11*, 835. (h) Li, C.; Lin, J. *J. Mater. Chem.* **2010**, *20*, 6831. (i) Wang, F.; Deng, R.; Wang, J.; Wang, Q.; Han, Y.; Zhu, H.; Chen, X.; Liu, X. *Nat. Mater.* **2011**, *10*, 968.

(3) (a) Bünzli, J.-C. G. *Chem. Rev.* **2010**, *110*, 2729. (b) Shen, J.; Sun, L.-D.; Yan, C.-H. *Dalton Trans.* **2008**, 5687. (c) Carlos, L. D.; Ferreira, R. A. S.; de Zea Bermudez, V.; Julian-Lopez, B.; Escribano, P. *Chem. Soc. Rev.* **2011**, *40*, 536. (d) Karhunen, U.; Jaakkola, L.; Wang, Q.; Lamminmäki, U.; Soukka, T. *Anal. Chem.* **2009**, *82*, 751. (e) Lemyre, J.-L.; Ritcey, A. M. *Chem. Mater.* **2005**, *17*, 3040. (f) Zhou, J.; Sun, Y.; Du, X.; Xiong, L.; Hu, H.; Li, F. *Biomaterials* **2010**, *31*, 3287. (g) Li, Z.; Zhang, Y. *Angew. Chem.* **2006**, *118*, 7896. (h) Moore, E. G.; Samuel, A. P. S; Raymond, K. N. *Acc. Chem. Res.* **2009**, *42*, 542. (i) Bouzigues, C.; Gacoin, T.; Alexandrou, A. *ACS Nano* **2011**, *5*, 8488.

(4) (a) Ehlert, O.; Thomann, R.; Darbandi, M.; Nann, T. *ACS Nano* **2008**, *2*, 120. (b) Heer, S.; Kömpe, K.; Güdel, H. U.; Haase, M. *Adv. Mater.* **2004**, *16*, 2102. (c) Sivakumar, S.; van Veggel, F. C. J. M.; Raudsepp, M. *J. Am. Chem. Soc.* **2005**, *127*, 12464. (d) Wang, F.; Xue, X.; Liu, X. *Angew. Chem., Int. Ed.* **2008**, *47*, 906.

(5) (a) Sabbatini, N.; Guardigli, M.; Lehn, J.-M. *Coord. Chem. Rev.* **1993**, *123*, 201. (b) Deng, K.; Gong, T.; Hu, L.; Wei, X.; Chen, Y.; Yin, M. *Opt. Express* **2011**, *19*, 1749. (c) Schietinger, S.; Aichele, T.; Wang, H.-Q.; Nann, T.; Benson, O. *Nano Lett.* **2010**, *10*, 134. (d) Boyer, J.-C.; Gagnon, J.; Cuccia, L. A.; Capobianco, J. A. *Chem. Mater.* **2007**, *19*, 3358. (e) Guo, H.; Li, Z.; Qian, H.; Hu, Y.; Muhammad, I. N. *Nanotechnology* **2010**, *21*, No. 125602. (f) Yi, G. S.; Chow, G. M. *Adv. Funct. Mater.* **2006**, *16*, 2324.

(6) (a) Mai, H.-X.; Zhang, Y.-W.; Si, R.; Yan, Z.-G.; Sun, L.-D.; You, L.-P.; Yan, C.-H. *J. Am. Chem. Soc.* **2006**, *128*, 6426. (b) Zhang, C.; Sun, L.-D.; Zhang, Y.; Yan, C.-H. *J. Rare Earths* **2010**, *28*, 807. (c) Wang, F.; Han, Y.; Lim, C. S.; Lu, Y.; Wang, J.; Xu, J.; Chen, H.; Zhang, C.; Hong, M.; Liu, X. *Nature* **2010**, *463*, 1061.

(7) Huang, Q.; Yu, J.; Ma, E.; Lin, K. *J. Phys. Chem. C* **2010**, *114*, 4719.

(8) (a) Li, Z.; Zhang, Y. *Nanotechnology* **2008**, *19*, No. 345606. (b) Wang, F.; Liu, X. *J. Am. Chem. Soc.* **2008**, *130*, 5642.

(9) (a) Chen, H.; Dong, S. *Langmuir* **2007**, *23*, 12503. (b) Wang, X.; Sun, Z.; Shao, C.; Boye, D. M.; Zhao, J. *Nanotechnology* **2011**, *22*, No. 245605.

(10) Mai, H.-X.; Zhang, Y.-W.; Sun, L.-D.; Yan, C.-H. *J. Phys. Chem. C* **2007**, *111*, 13721.

(11) Aebischer, A.; Hostettler, M.; Hauser, J.; Krämer, K.; Weber, T.; Güdel, H. U.; Bürgi, H.-B. *Angew. Chem., Int. Ed.* **2006**, *45*, 2802.

(12) Mironov, V. S. *Spectrochim. Acta, Part A* **1998**, *54*, 1607.

(13) Abel, K. A.; Boyer, J.-C.; Andrei, C. M.; van Veggel, F. C. J. M. *J. Phys. Chem. Lett.* **2012**, *2*, 185.